7622–7632 Nucleic Acids Research, 2012, Vol. 40, No. 16 Published online 1 June 2012
doi:10.1093/nar/gks517

A large-scale association study for nanoparticle C60 uncovers mechanisms of nanotoxicity disrupting the native conformations of DNA/RNA

Xue Xu[1], Xia Wang[1], Yan Li[2], Yonghua Wang[1,*] and Ling Yang[3]

[1]Center of Bioinformatics, College of Life Science, Northwest A&F University, Yangling, Shaanxi 712100, China, [2]School of Chemical Engineering, Dalian University of Technology, Dalian 116024, Liaoning and [3]Laboratory of Pharmaceutical Resource Discovery, Dalian Institute of Chemical Physics, Chinese Academy of Sciences, Dalian 116023, China

Received April 3, 2012; Revised May 5, 2012; Accepted May 9, 2012

ABSTRACT

Nano-scale particles have attracted a lot of attention for its potential use in medical studies, in particular for the diagnostic and therapeutic purposes. However, the toxicity and other side effects caused by the undesired interaction between nanoparticles and DNA/RNA are not clear. To address this problem, a model to evaluate the general rules governing how nanoparticles interact with DNA/RNA is demanded. Here by, use of an examination of 2254 native nucleotides with molecular dynamics simulation and thermodynamic analysis, we demonstrate how the DNA/RNA native structures are disrupted by the fullerene (C60) in a physiological condition. The nanoparticle was found to bind with the minor grooves of double-stranded DNA and trigger unwinding and disrupting of the DNA helix, which indicates C60 can potentially inhibit the DNA replication and induce potential side effects. In contrast to that of DNA, C60 only binds to the major grooves of RNA helix, which stabilizes the RNA structure or transforms the configuration from stretch to curl. This finding sheds new light on how C60 inhibits reverse transcription as HIV replicates. In addition, the binding of C60 stabilizes the structures of RNA riboswitch, indicating that C60 might regulate the gene expression. The binding energies of C60 with different genomic fragments varies in the range of −56 to −10 kcal mol^{-1}, which further verifies the role of nanoparticle in DNA/RNA damage. Our findings reveal a general mode by which C60 causes DNA/RNA damage or other toxic effects at a systematic level, suggesting it should be cautious to handle these nanomaterials in various medical applications.

INTRODUCTION

Without a doubt, nanotoxicology has to mature as a scientific discipline to enable the widespread application of nanoparticles (1). Despite the early acceptance and rapid progress of nanoparticle toxicity assessments, the potential toxic mechanisms of interactions between the nanoparticles and the biological systems have not yet been fully elucidated. Studies on the interactions of the nanoparticles and proteins/nucleic acids may provide guidance for understanding the basic questions in nanotoxicology.

Most of the studies have so far focused on changes in the protein structure or local or global changes in protein dynamics upon binding to nanoparticles. Single-walled carbon nanotubes (SWNTs) are found to plug into the hydrophobic core of protein WW domains to disrupt and block the active sites, which finally leads to the loss of the original function of protein (2). Similar effects have also been observed with the irreversible gold nanoparticles (AuNP)-induced conformational changes of human ubiquitin (hUbq) protein (3). Separately, it is also shown in our recent work that fullerene C60 adsorbs onto the cell-membrane P-glycoprotein through hydrophobic interactions, but the stability and secondary structure of the protein are barely affected (4). Also, we note the strong association of C60 molecules with ion channels, enzyme and antibodies where the binding depends on the particle size and native protein structures (5).

Despite the extensive studies in the nanoparticle–protein hybrids, to date, the 'substantive nature' of the

*To whom correspondence should be addressed. Tel: +86 029 87092262; Fax: +86 029 7091175; Email: yh_wang@nwsuaf.edu.cn

The authors wish it to be known that, in their opinion, the first two authors should be regarded as joint First Authors.

effects of nanoparticles on nucleic acids has only been partially clarified. The nano studies are limited by the fact that researchers mainly focus on the hybrids of carbon nanotubes with DNA sequences in most cases. For example, poly(GT) DNA sequences are shown to be rolled up onto SWNTs to form stable barrels, which results in structures analogous to the well-known protein β-sheet motifs (6). Through molecular simulation (MD) studies, single-stranded DNA (ssDNA) has been found to form right-handed helical wraps around the outside of SWNTs, dependent on both the DNA sequence and the SWNT chirality (7). In our previous work, we also found the unique wrapping behaviors of chiral and armchair SWNTs by DNA dinucleotides that display base flipping, local dynamic stability of structure and conformational shifting (8). The resulting structural destabilization and deformation of the DNA sequences imply that the nanomolecules probably exert certain toxic effects in organisms, which is very different from the traditional large-scale materials.

The molecular recognition features of carbon nanotubes with DNA are somewhat clarified at the moment; while for another carbon nanomaterial C60, one of the most important nano-drug carriers, its interaction mechanism with DNA/RNA are still illusive. Indeed, a pioneering study has found that C60 binds tightly to DNA and speculated that this association may negatively impact the self-repairing process of the double-stranded DNA (dsDNA) (9). Nonetheless, several fundamental questions still remain unclear due to the restrictions associated with the earlier disadvanced computing facilities. For example, whether RNA hybridizes to C60? What is the structural basis for the DNA/RNA recognition of C60 particle? Could the native structures of DNA/RNA be disrupted by C60 binding? Do the hybrids of DNA/RNA with C60 bear any biological relevance that leads to the potential nanotoxicity?

In this study, we report the static and dynamic bindings of DNA/RNA to C60 by using geometry-based algorithm and molecular dynamics (MDs) simulations, and find that the nanomolecule enables to disrupt the native conformations of these fragments. Further thermodynamic analysis verifies our results, and explains the specific hybrids between C60 and nucleotide fragments from the energy aspect.

MATERIALS AND METHODS

Preparation of structure-based test set

To investigate the binding properties of C60 with nucleotides, a total of 2254 animal and bacteria nucleotide samples were selected from the Nucleic Acid Database (NDB) to achieve the most extensive sampling (http://ndbserver.rutgers.edu/index.html, accession time: February 23, 2012), which consisted of four sets of crystal structures, including ligand–DNA/RNA complexes and free DNA/RNA structures. A nucleic acid fragment was selected according to the following criteria: (i) selecting the structure without artificial mutations (e.g. PDB codes 1CS7, 1PUY and 265D) or cleavages (e.g. PDB codes 1F6C, 1P24 and 2FII) around the binding site where C60 binds based on the geometry-based algorithm and (ii) deleting the ssDNA (e.g. PDB codes 1G6D, 1QYK and 382D). Finally, 589 ligand–DNA complexes yielded a total number of 313 cases, while 432 ligand–RNA complexes formed a set of 230 cases. For the 767 free-DNA fragments and 466 free-RNA fragments, 193 and 166 cases were generated according to the above selection criteria, respectively (the PDB codes for the selected structures can be seen in Supplementary Data). All these structures were manually inspected using VMD 1.9.1 (10) and PyMOL v1.4 (http://www.pymol.org/).

Binding modes and dynamics of nucleotides

Geometry-based algorithm (11) was applied to identify the binding modes of C60 with the nucleic acid strands that were treated as rigid bodies. This method employed three-dimensional transformations driven by local feature matching, and spatial pattern detection techniques, such as the geometric hashing and pose clustering, to yield good molecular shape complementarity with high efficiency. After the fast transformational search, the best geometric fit obtained the highest scores (~5000), while the low scores (~500) exhibited poor matches. For the complexes in our work, the clustering root mean square deviation (RMSD) was 4 Å. The 5 lowest binding energy matches for each complex were selected and analyzed visually.

To analyze the dynamics of nucleotides under physiological conditions, each complex was further simulated with MD using the GROMACS 4.5.1 MD package (12) on a simulation time scale of 70 ns. These structures were solvated in triclinic boxes with box vectors of ~10 Å length. The systems were energy minimized, followed by a relaxation for 400 ps, with positional restraints on the DNA/RNA atoms by using a force constant of $k = 1000\,\mathrm{kJ\,mol^{-1}\,nm^{-2}}$. The CHARMM27 force field (13) with CMAP corrections (14) was used for the nucleic acid and SPC/E for the water model (15). All simulations were performed in the NPT ensemble. The temperature was kept constant by Nose–Hoover temperature coupling at $T = 300\,\mathrm{K}$, with a coupling time of $T_p = 0.5$ ps (16). The pressure was coupled to a Parrinello–Rahman with $T_p = 4$ ps and an isotropic compressibility of $4.5 \times 10^{-5}\,\mathrm{bar^{-1}}$ in the x, y and z directions (17). All bonds were constrained with the LINCS algorithm (18). Electrostatic interactions were calculated explicitly at a distance smaller than 10 Å; long-range electrostatic interactions were calculated by particle mesh Ewald method, with a grid spacing of 0.12 nm and fourth order B-spline interpolation (19). Structures were written out every 10 ps for subsequent analysis.

Calculation of binding affinity

The calculation of binding free energies for the C60–DNA and C60–RNA complexes was evaluated using MM-GBSA (molecular mechanics general Borned surface area) method (20,21). This approach employed molecular mechanics, generalized Born model and solvent accessibility method to elicit the free energy from the structural information circumventing the computational complexity of the free-energy simulations. It was parametrized within

the additivity approximation (22) wherein the net free-energy change was treated as a sum of a comprehensive set of individual energy components, each with a physical basis. Briefly, in the MM-GBSA approach, the C60–DNA/RNA binding free energy ($\Delta G_{binding}$) for each snapshot was estimated as

$$\Delta G_{binding} = \left[G_{complex}\right] - \left[G_{DNA/RNA}\right] - \left[G_{C60}\right] \quad (1)$$

The free energy of each of the above terms was calculated from

$$\Delta G_{tot} = \Delta E_{MM} + \Delta G_{solv} - T\Delta S \quad (2)$$

where E_{MM} is the molecular mechanics energy of the molecule expressed as the sum of the internal energy (bonds, angles and dihedrals) (E_{int}), the electrostatic energy (E_{ele}) and van der Waals (E_{vdW}) terms. For the unique nanoparticle C60, its E_{int} and E_{ele} equal to 0 kcal mol^{-1}. G_{solv} accounts for the solvation energy, which can be divided into the polar and nonpolar parts. Obtaining the solvation free energy (G_{solv}) from an implicit description of the solvent as a continuum is advantageous because it affords a solvation potential that is only a function of the solute's geometry, as discussed and implemented by Srinivasan *et al.* (23). As reported by our previous studies (8), the contribution of the entropy ($T\Delta S$) was negligible because the difference of $T\Delta S$ was very small considering the similarity of the systems.

RESULTS AND DISCUSSION

It is known that DNA/RNA fragments possess complex structural features such as high density charge and helix chiral geometry, and do not present a single and well-defined binding site. For the nanoparticle C60, this unique molecule shapes like a hollow sphere and behaves chemically and physically as electron-deficient alkenes, thus probably eliminating more interferences from the nucleic acid specificity and identifying their potential targets. In addition, for most of the successful drugs targeting the nucleic acids, they are organic molecules such as the aromatic and heterocyclic compounds, which enable to form noncovalent or covalent interactions in the grooves with different sequence selectivity. This is overwhelmingly favorable for C60 to interact with the nucleic acids due to its benzene-derived ring structure. Indeed, previous studies have already shown the unique carbon nanotube–DNA hybridization modes with an emphasis on the structural deformation of nucleotides (6–8). However, it is still unclear whether and how C60 binds to DNA/RNA, and do the hybrids produce serious toxic effects on nucleotides?

Static hybridization of C60 with DNA

To address this, we begin our study by simulating the binding of C60 with the dsDNAs derived from the ligand–DNA crystal structures that show the representative properties of nucleotide segments. Figure 1A shows 205 interactions of C60 with the base pair guanine and cytosine (C60-guanine–cytosine; C60GC), in which 118 (48.0%) involve three consecutive GC base pairs ($C60GC_3$). Of the 129 complexes, where the binding sites of C60 contain the base pair adenine and thymine (AT), there are only 42 structures (17.1%) encompassing three consecutive AT base pairs ($C60AT_3$) (Figure 1A). These results indicate that C60 selectively binds to the GC base pair compared with the AT base pair.

Further analysis shows that C60 has varying degrees of groove preference for different sequences (Figure 1A), i.e. the $C60GC_3$ binding mode occurs far more often in the minor grooves (41.1%), while the $C60AT_3$ mode display a higher preference for the major grooves (13.4%). More strikingly, for those binding modes where the base pairs GC and AT coexist, i.e. C60GC-GC-AT, C60GC-AT-GC, C60AT-GC-AT and C60AT-AT-GC, the C60 molecule is found to bind to the DNA segments with the same preference for the major grooves as the $C60AT_3$ mode, which indicates a significant role of the base pair AT in determining the groove binding specificity of C60.

The binding of ligand probably alters the native conformations of free nucleotide fragments, thus leading to certain changes in C60 binding modes. In order to eliminate this, we further collected 193 crystal structures of free-dsDNA segments from NDB to analyze their interactions with C60 and to compare the binding modes with those of ligand-bound complexes. As shown in Figure 1B, C60 shows the same preference for the $C60GC_3$ binding mode (>36%), whereas the proportions of $C60AT_3$ binding mode are still found to be very low (<18%), supporting our idea that C60 has a strong tendency to bind to the GC-rich regions of nucleotides. Also, the hybrids of C60 molecule with the three consecutive GC or AT base pairs of free-dsDNA segments are found to display the same preference for the minor or major grooves (77.1 and 66.7%, respectively). Screening of the free-DNA segments obviously vouches for the accuracy of our modes, and meanwhile, reveals the potential C60 binding targets of interest for biological and pharmacological activity.

Consequently, the above observations raise a question of why C60 prefers to hybrid with the GC_3 sequences in the minor grooves. In fact, it has been reported that the GC-rich regions of nucleotides have a strong tendency to be minor groove wide (width >5 Å), while the AT-rich DNA tend to be minor groove narrowing (width <5 Å) (24), which suggests the sequence dependence of minor groove width. As C60 molecule shapes like a hollow sphere with a diameter of 7.0 Å, larger than the minor groove width of AT-rich regions, it is thus reasonable to believe that this nanoparticle tends to bind to the wider minor grooves along the GC sequences.

To further investigate the binding preference of C60, we select four representative systems from the C60GC3 and C60AT3 binding modes to estimate their binding free energies, respectively (Table 1). It is worth to note that since the C60 in our systems carries no charge, the contribution of the electrostatic energy is neglected. The results show that the systems in the C60GC3 mode have much lower G_{total} (nearly 6 kcal mol^{-1}) than those in the C60AT3 binding modes, indicating the more favorable interactions of the C60 molecule with the GC-rich

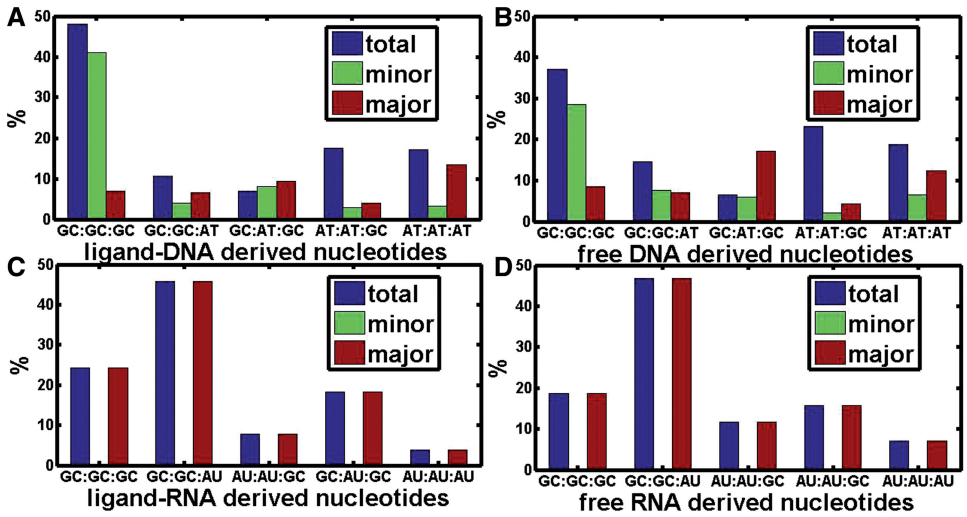

Figure 1. Static hybridization characteristics of C60–DNA/RNA complexes. (**A** and **B**) show percentages of nucleotide sequences derived from the ligand–DNA and free-DNA crystal structures that hybrid with C60 in the GC:GC:GC, GC:GC:AT, GC:AT:GC, AT:AT:GC and AT:AT:AT regions, respectively. (**C** and **D**) show those from ligand–RNA and free-RNA structures that hybrid with C60 in the GC:GC:GC, GC:GC:AU, AU:AU:GC, GC:AU:GC and AU:AU:AU regions, respectively. Blue color represents the total percentages of C60–DNA/RNA recognition; cyan the percentages of minor groove recognition; red the percentages of major groove recognition, respectively.

Table 1. Calculation of binding free energy for static hybridization of C60 with DNA/RNA

Nucleic acid	Binding sites	System	E_{vdW}		G_{solv}		G_{tot}	
			Mean (kcal mol^{-1})	Standard deviation	Mean (kcal mol^{-1})	Standard deviation	Mean (kcal mol^{-1})	Standard deviation
DNA	GC:GC:GC	1IH1	−33.51	5.07	7.89	0.96	−25.62	2.57
		461D	−32.90	2.01	7.43	0.87	−25.47	1.86
	AT:AT:AT	2V3L	−14.80	1.79	5.04	0.94	−9.76	1.33
		432D	−32.49	2.59	8.99	0.81	−23.50	2.12
RNA	GC:GC:GC	1F79	−33.39	6.37	15.87	2.02	−17.52	5.04
		1KD4	−10.73	1.33	4.16	0.85	−6.56	1.01
	GC:GC:AU	1F7I	−36.43	3.86	15.32	1.59	−21.10	2.90
		1Y99	−48.60	2.77	21.28	2.18	−27.33	2.47
	GC:AU:GC	3NJT	−11.61	1.84	4.88	0.78	−6.73	1.34
		2NOK	−33.53	6.56	14.89	2.44	−18.63	4.51
	AU:AU:GC	1LNT	−34.22	3.45	18.40	2.94	−15.82	2.25
		2KU0	−26.45	2.52	10.69	1.09	−15.76	1.90
	AU:AU:AU	1YY0	−36.55	5.95	15.54	2.55	−21.01	3.88
		3S49	−33.85	2.44	12.17	0.88	−21.68	1.95

regions of DNA. This thus further explains why C60 prefers for the minor grooves of the GC sequences to some extent.

Static hybridization of C60 with RNA

Next, we have investigated the molecular recognition features of RNA after the hybridization. As shown in Figure 1C, C60 prefers for the GC-rich regions of RNA, especially the GC-GC-AU sequences that contain ~2.6–9.8 times the number of AT-rich sequences. Most strikingly, the nano molecule C60 binds only to the major groove sites of RNA, and no association has been observed at the minor groove sites in our simulations, as shown by the blank cyan plots in Figure 1C. Since the major groove of RNA (12.9 Å) is much deeper compared to its minor groove (3.3 Å) (25), we expect that the depth of the RNA grooves greatly impacts the accommodation of C60, and finally leads to the extremely high tendency of C60 hybrids for the major grooves.

To further evaluate the binding tendency of RNA, we choose two representative C60–RNA complexes from each of the modes to calculate their binding energies. The data in Table 1 show that the binding energies vary considerably with different base sequences. The systems in the C60GC-GC-AU mode have binding energies of ~ −24 kcal mol^{-1}. While for the systems containing two or three AU base pairs, the changes in sequences give relatively larger increases in the G_{total}, 3–9 kcal mol^{-1}. For systems in the C60GC-GC-GC and C60GC-AU-GC modes, the binding energies become more positive than

those of the systems in the C60GC-GC-AU mode (12 kcal mol^{-1}). Since lower binding affinities imply more stable binding of the ligands, the analysis of binding affinity of the C60–RNA complexes provides strong evidence for the preference of the nanoparticle for the GC-GC-AU sequences of the nucleotides.

Finally, we select 166 free-RNA structures from the NDB to enable the unbiased statistics. The results show similar preferences for C60 to hybrid with RNA (46.8% for the GC-GC-AU sequences) (Figure 1D). Moreover, the nanomolecule is still found to only hybrid with the major groove regions of RNA. These results confirm the accuracy of our modes, and imply that the hybridization features of C60 depend on the nature of the nucleotides.

Hybridization-induced structural changes in DNA/RNA

The above observations provide new insight into the recognition of DNA/RNA by C60. These models, however, also reveal a lack of realistic circumstance for the C60 hybridization, and little consideration to the issue of the dynamics of DNA/RNA. Toward the next level of understanding, we thus investigated the hybridization-induced structural changes of DNA/RNA using MD simulations.

DNA

dsDNA twist. The C60-induced twist on dsDNA is firstly observed, which accounts for 17% of the total C60–DNA dynamic interaction systems (e.g. PDB codes 1XRW, 1CYZ, 1QSX, 378D and 245D). As shown in Figure 2A (PDB code 1XRW), the C60 molecule is initially located at the GC:GC binding site where the minor groove of the DNA faces the nanomolecule surface. After 1–2 ns, the C60 slides along a linear path, parallel to the DNA axis, with distance of ~8 Å to the neighboring AT:GC site, and sticks to the site for the rest of the simulation time (50–60 ns) (Figure 2B). During the process, significant conformational changes of the DNA sequence occur, showing an anti-clockwise twist of the nucleotide along its helix-parallel axis (~40°) with respect to its initial position.

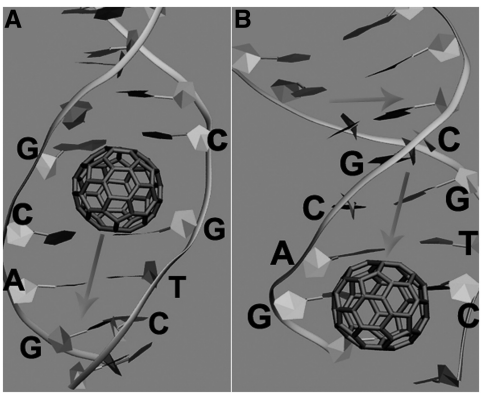

Figure 2. Interactions of C60 with dsDNA in the 1XRW system. (**A**) The binding of C60 to the DNA at GC:GC binding site, and (**B**) shows the sliding of the nanoparticle to the GC:AT site. The arrows show the sliding directions of the C60 molecule and the rotation direction of the DNA fragment.

Comparison of the MD trajectory with the static C60–DNA hybridization mode reveals a difference between the initial identified site of C60 (the GC:GC:AT binding region obtained from the geometry-based algorithm) and its final stabilized site (the AT:GC binding region obtained from the MD simulation). This interesting change might be similar to the process of food intake by mouth (initial) and then digestion in stomach (final). Detailed analysis of the final stabilized sites for all the C60–DNA systems is given in Section "Statistical analysis of dynamic hybridization".

Evidently, these sequences in the sliding-induced twist mode share a unique binding region that is composed of two successive GC:GC or AT:AT base pairs and the following AT:GC base pairs. In fact, the above analysis of static hybridization has described the direct binding of C60 with the GC:GC or AT:AT sites on the basis of the geometric fit. Such hybrid, however, exhibits an unstable state in the MD simulations due to the asymmetry of the GC or AT repeats, and thus causes the sliding of the C60 molecule and the subsequent conformational changes of the dsDNA fragments.

dsDNA unwinding. Another intriguing finding is that the binding of C60 has high probability for triggering the initiation of DNA unwinding, accounting for 32.1% of the total systems. For example, C60 interacts with the GC:AT site of DNA through hydrophobic interactions in the initial 4 ns (Figure 3A). Then, the nanomolecule slides along the DNA helix to the neighboring base pairs GC:GC with a distance of 6 Å, and stays in the location for ~45 ns (Figure 3B). Due to the dynamic instability induced by the C60 binding, the nanomolecule slides rapidly back to the AT:GC site again. Almost immediately, the AT:AT sequence in the 3′-terminal undergoes a torsion deformation involving the outward tilting of T1 and T2 (~100°) and the rotation of A7 and A8 (~30°), which finally leads to the partial unwinding of the DNA fragment (Figure 3C).

Two types of DNA sequence properties that correlate with the unwinding mode are identified in this section: (i) For the AT:AT:$(GC)_3$ sequences, such as the structures with the PDB codes of 1CP8, 1QCH and 2D55, C60 initially binds to the AT:GC site, and then slides to the third GC base pair. After return to the AT:GC site, the binding site is forced to unwind. (ii) For the GC:GC:AT:AT(GC) sequences, such as the structures with the PDB codes of 1I5V and 1MPT, C60 interacts with the GC:GC region in the first 3 ns and subsequently slides along the DNA helix to the neighboring AT:AT or AT:GC sites. After a transient pause (~5–15 ns), the small molecule relocates at the GC:GC region, and finally induces the partial unwinding of this site.

It is known that Okazaki fragments are newly synthesized DNA fragments that are formed on the lagging template strand during the DNA replication, and are short molecules of ssDNA between 100 and 200 nt long in eukaryotes (26). Since our results show the unwinding mode of DNA fragments when hybridized with C60, it is reasonable to speculate that the binding of C60 molecule could inhibit the DNA discontinuous

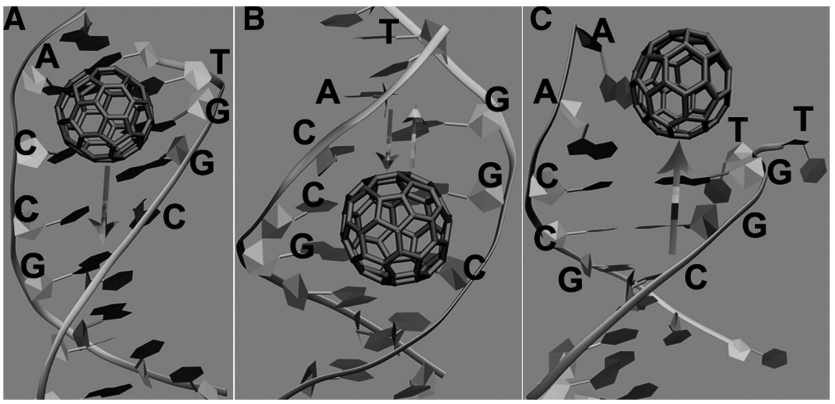

Figure 3. Interactions of C60 with dsDNA in the 1CP8 system. (**A** and **B**) show the binding of C60 to the DNA at AT:GC binding site, and the subsequent sliding to the GC:GC site, respectively. (**C**) The unwinding of the dsDNA fragment. The arrows show the sliding directions of the C60 molecule.

replication by disrupting the structures of Okazaki fragments and lagging the strand template. This thus should raise great concerns about the introduction of nanoparticles in the therapeutic fields.

dsDNA stability. Evidence from MD simulations (e.g. PDB codes 108D, 1AMD, 1MTG, 1N37, 1RQY, 2ADW, 2GWA and 3GSK) shows that the binding of C60 has little or no effects on the conformations of DNA fragments involving the AT:GC:GC(AT) sequences, which accounts for 32% of the total C60–DNA complexes. Figure 4 shows that the C60 molecule intercalates into the AT:GC base pairs with the plane of the aromatic nucleotide bases oriented parallel to the surface of the nanotube, and maintains such binding mode through the entire 70 ns simulation. Since the π–π stacking interactions of C60 with the DNA fragment contribute most to the complex stability, and this type of directional force is comparable in strength to hydrogen bonding and can, in some case, be a decisive intermolecular force, we believe that the strong stacking is the key to this phenomenon, in which the nucleic acid fragment maintains its rigidity upon the binding of C60.

Indeed, among the main DNA binding modes, intercalation is proposed to be the most common way through which small and rigid aromatic molecules recognize the DNA (27). However, since the binding of intercalators to DNA depends basically on π-stacking and electrostatic interactions, most of the ligands possess less sequence specificity, which is a major obstacle to the target recognition. In this section, we have found the DNA–C60 interactions and the resulting intercalation structure is dependent on both the DNA sequence and the C60 structure. This points to the possibility of selecting C60 for specific DNA sequence recognition.

G-quadruplex disruption. DNA is polymorphic, and can adopt diverse structures other than the Watson–Crick duplex when actively participating in the replication, transcription, recombination and damage repair (28). Of particular interest are guanine-rich regions, which present a non-canonical four-stranded topology, called the G-quadruplex. Such architecture involved in the 3′-overhang of telomeres of human chromosomes enables to block the catalytic reaction of the telomerase, a relevant target in oncology.

Figure 5A shows an example of the hybrid of C60 with the G-quadruplex DNA fragment in the wide groove (PDB code: 2JT7). The nanomolecule remains stable with no significant changes in orientation during the entire simulation (Figure 5D). In contrast, the bases T6 and T1 of the DNA fragment exhibit large tilts (∼90°) due to the attraction of C60-induced π–π stacking (Figure 5B), and finally form a 'sandwich' state with the nanomolecule, i.e. the C60 is clipped between T1 and T6 (Figure 5C). Scanning of all the trajectories in the G-quadruplex disruption mode confirms our results, and suggests that C60 enables to bind into the hydrophobic grooves of the G-quadruplex in a sidewise approach, but also stacks on the surface of the terminal quartet in an external mode. Despite the target disparity of C60, all the structures of G-quadruplex DNA fragments display great deformation after hybridization, which accounts for 9.2% of the total systems.

It is known that in normal somatic cells, telomere length decreases at each round of division and consequently these cells have a finite lifetime. While in human tumor cells, the reverse transcriptase enzyme telomerase is activated to maintain the telomere length so that tumor cells are effectively immortalized (29). Since the formation of a G-quadruplex structure at the 3′-end of telomeric DNA effectively hinders the telomerase from adding further repeats, we speculate that C60 that disrupts the G-quadruplex could activate the telomerase by facilitating its access to the telomeres and could therefore induce potential side effects of therapeutic treatments when C60 was used as anticancer drug carriers.

RNA

RNA curling. After being perceived for a long time merely as an intermediate between DNA (the depository of the genetic information) and proteins (the macromolecules that work inside a cell), RNA now is the center of attention in biomedical research. RNA's boost in fame is

partially attributable to the discovery of its role in being an integral part of many biological processes.

In this section, we find a structural transition of RNA between two states, the RNA stretch state and the RNA curling state, and such transition only exists in the HIV trans-activating region (TAR) RNA fragments (e.g. PDB codes: 1AKX, 1ARJ, 1LVJ, 1QD3 and 1UTS, accounting for 9.5% of the total). The dynamics of the stretch→curling transition, monitored using time-dependent changes in RMSD of the RNA, shows that the molecules undergo specific transitions at ~10 ns, and spend a substantial fraction of time (~60 ns) in the curling state (Figure 6D). Since the transition involves the formation of intersubunit contacts, we take the TAR RNA in the 1AKX system as an example to dissect the transition.

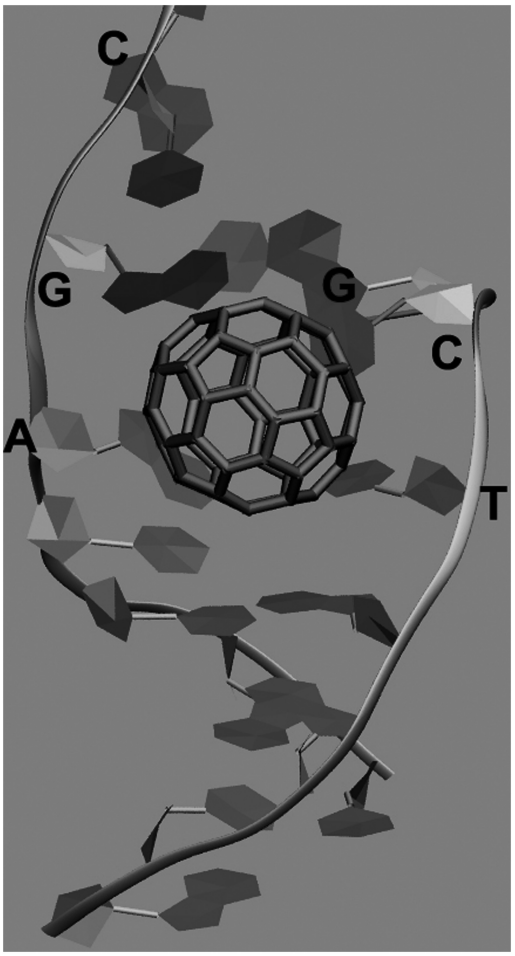

Figure 4. Binding of C60 to the dsDNA at GC:AT binding site in the 108D system.

Upon the binding of C60, the two bases A22 and U23 capture the nanomolecule via π–π stacking interactions and remain constant during the entire simulation (Figure 6A). This event accompanies the significant fluctuation of A35 as evidenced by its large rotation of angle (CB-CG-CD-CE) from −180° to ~180° (Figure 6B and E). Subsequently, the G33 in the middle of the stem region has tilted by ~50° (CD-ND-CA-CB) to form π-stacking with the C60 molecule (Figure 6C). Coupled with the significant conformational change of G33, the loop region is forced to undergo the upward curling and maintain the state for ~30 ns as evidenced by the torsional rigidity of G33 and A35 (from ~40 ns to ~60 ns) (Figure 6E).

Indeed, the interaction between positive transcription elongation factor complex b (P-TEFb), Tat protein and TAR is a key step in the transactivation process of HIV-1, and TAR RNA is shown to exhibit specificity to P-TEFb–Tat-TAR complex formation (30,31), which implies the major role of TAR RNA molecule in assembling a regulatory switch in HIV replication. Thus, we speculate that the structural changes of the TAR RNA induced by C60 could disrupt the structural association of the RNA molecule with its protein partners, resulting in inhibiting the HIV reverse transcription and repressing the expression of HIV.

Riboswitch stabilization. Riboswitches have been reported to be capable of binding cellular metabolites using a diverse array of secondary and tertiary structures to modulate the gene expression (32). Results of the MD simulations (e.g. PDB codes: 2HOK, 2H0M, 3NPB, 2YDH and 2GIS, accounting for 19.5% of the total) show that the C60 molecule presents a similar binding mode as those of riboswitch substrates, and enables to stabilize the conformations of riboswitches.

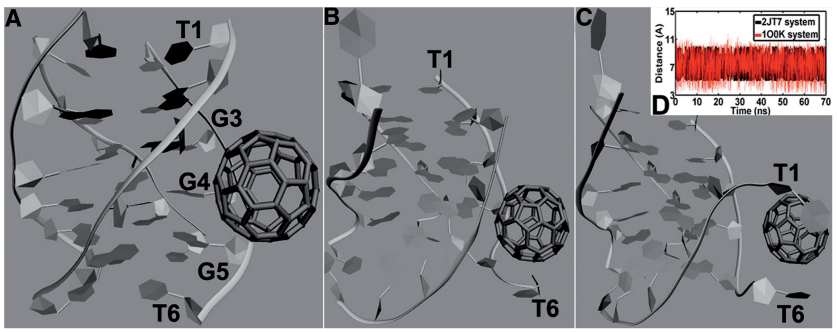

Figure 5. Interactions of C60 with G-quadruplex DNA in the 2JT7 system. (**A–C**) show the conformational changes of G-quadruplex with the binding of C60. (**D**) shows the time evolutions of the distance between the G-quadruplex DNA fragment and C60.

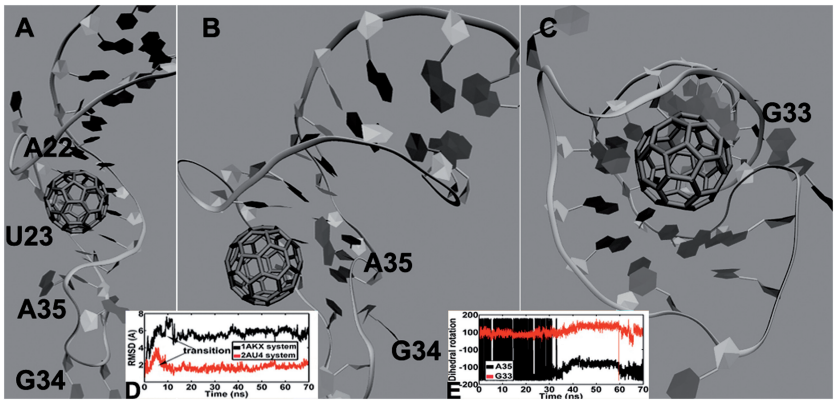

Figure 6. Interactions of C60 with double-stranded RNA in the 1AKX system. (**A–C**) show the conformational changes of dsRNA with the binding of C60. (**D**) The RMSD of dsRNA versus simulation time in the 1AKX and 2AU4 systems. (**E**) reveals the time-dependent rotation of G33 and A35 about the (CD-ND-CA-CB) and (CB-CG-CD-CE) dihedral angles, respectively.

For example, the SAM-I riboswitch is based around an elaborated four way helical junction (PDB code: 3NPB). Several nucleic acids (notably C48, G79 and A111) in the P1 and P3 helices, and the intervening J1/2 and J3/J4 joining regions of the junction interact with the C60 molecule thus creating a ligand binding pocket (Figure 7A). This nanomolecule constantly sticks to this binding site during the entire simulation (Figure 7B). More interestingly, in the presence of C60, the riboswitch is found to engage in the same conformation as the binding of substrate *S*-adenosylmethionine, thereby probably maintaining the folding of the expression platform (33). Since the conformations of the expression platform direct the transcriptional or translational controls, the C60 has great potential to be a new type of riboswitch substrate to regulate the gene expression.

dsRNA stabilization. It is commonly accepted that molecular recognition and formation of the noncovalent complex are driven by non-specific interactions and sequence-specific structural features along the major groove of RNA (28). Figure 8A shows that the C60 molecule locates at the major grooves of RNA and displays a modest selectivity for G-rich regions involving at least four G bases (e.g. PDB codes: 1BYJ, 1EI2, 2JUK, 2FCX and 1FYD), which accounts for 35.6% of the total systems. Once the binding sites have been identified, the C60 molecule rapidly slides along the major groove (Figure 8C). At ~25 ns, this molecule turns out of the groove to form a relatively stable complex through hydrophobic interactions via its hydrophobic surface and the end of the RNA strand (Figure 8B). Interestingly, during the whole MD simulations, we do not observe evident conformational changes of the RNA fragments.

Since DNA with high GC content is more stable than DNA with low GC content (34), it is possible that the G-rich RNA sequences also adopt stable conformations in spite of the interferences induced by the C60 hybridization. This indicates that the structural stability of dsRNA relies on sequence specificity of nucleotides.

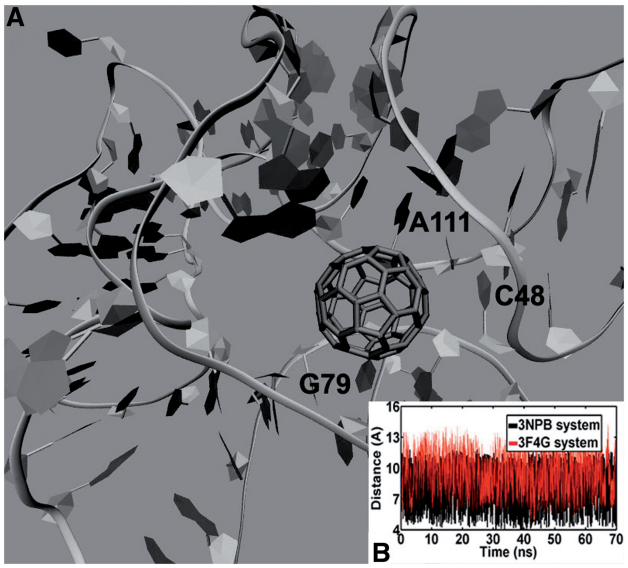

Figure 7. (**A**) Interactions of C60 with riboswitch RNA in the 3NPB system. (**B**) Time evolution of the distance between C60 and the riboswitch RNA fragment in the 3NPB and 3F4G systems.

Statistical analysis of dynamic hybridization

In this section, we have statistically analyzed the final stabilized sites of C60 in all the C60-dsDNA/dsRNA dynamic interaction systems, and compared these sites with the initial identified sites (Figure 1). Figure 9 shows the four or three types of the hybridization modes of C60 with DNA/RNA. For the C60-DNA hybrids, the nanomolecule is significantly preferred over the GC:AT sites (40.8%). Although the specific recognition of minor/major groove and the intercalation by C60 are found in almost all DNA hybridization modes (GC:AT, AT:AT and GC:GC), their preference in each can vary dramatically. The GC:AT regions have a relatively high percentage of 28.6% to form stronger hydrophobic interactions with C60 in the minor grooves. Contrary to this, the AT:AT and GC:GC regions have comparatively low

minor groove-recognition percentages of 7%, but high percentages of 13% to hybrid with C60 by intercalating. In the case of the C60-RNA hybrids, GC:AU sites are highly favored over GC:GC regions (56.2% versus 18.7%), and show a strong preference for the major grooves.

These results show the substantial differences between the final stabilized sites of C60 and its initial identified sites, which suggest the sequence-specific changes in realistic physiological circumstances.

Binding energy analysis

The above sections have revealed the dynamic interactions of DNA/RNA with C60, and indicated seven unique types of nucleotide conformations. Such observations strongly indicate that the different interaction interfaces and binding specificity of nucleotides may be coupled to binding energies with enormous disparities. To examine the hypothesis, we have thus selected two representative systems from each binding mode, and estimated their binding free energies with C60, respectively.

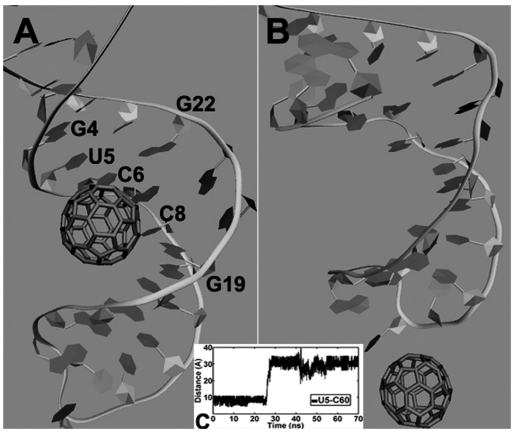

Figure 8. (**A**) Interactions of C60 with double-stranded RNA in the 1BYJ system. (**B**) Time evolution of the distance between C60 and U5. (**C**) The time evolution of the distance between the base U5 and the C60 molecule.

The data in Table 2 show the much higher binding affinities (~10 kcal mol^{-1}) of nucleotides in the dsDNA/riboswitch stabilization and G-quadruplex disruption modes compared with those in the other hybridization models. Indeed, the C60 is found to constantly stick to the nucleotides and remain in the stable state through the whole simulation time in the above three modes. Under such condition, the surface of nanomolecule provides more spaces for the hybrids of DNA/RNA, therefore aggrandizing the vdW interaction (~43 kcal mol^{-1}). In contrast, the nucleotides in the dsDNA twist, dsDNA unwinding, dsRNA curling and dsRNA stability modes display much weaker vdW energies (~30 kcal mol^{-1}). This is quite reasonable since the large and flexible movement of these nucleotides enables to induce their less favorable interactions with C60.

In addition, we notice that the C60 hybridization in all cases is accompanied by the reduction of solvent accessible surface area (SASA) due to the burial of large portions of C60 surface through the stacking of DNA bases, thus leading to a comparatively large, negative contribution of the solvation free energies (G_{solv}) to the binding free energy. Closer inspection reveals that the systems in the dsDNA twist, dsDNA unwinding, dsRNA curling and dsRNA stability modes have relatively smaller G_{solv} (3–5 kcal mol^{-1}) than those in the other binding modes. Indeed, the C60 molecule has displayed different sliding movements along the DNA/RNA axis in the above four modes. Such unique motions probably significantly decrease the SASA during the simulations, and thereby lead to the smaller G_{solv}.

Surprisingly, further comparison of the C60-nucleotides binding affinities in the initial identified sites with those in the final stabilized sites demonstrates a 2-fold difference (Table 2), which implies that the hybrid-induced dynamics of nucleotides significantly affects the hybridization modes of C60, quite similar to the food intake process from the mouth to the stomach.

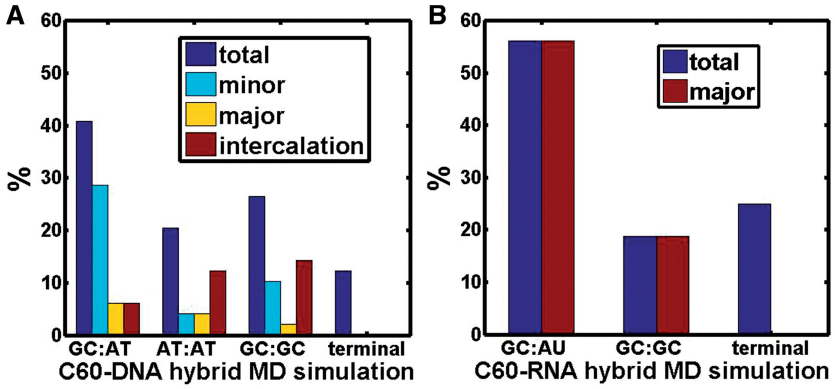

Figure 9. Dynamics hybridization characteristics of C60-DNA/RNA complexes. (**A**) shows the percentages of representative DNA sequences derived from the MD simulations that hybrid with C60 in the GC:AT, AT:AT, GC:GC and terminal regions, respectively. (**B**) The percentages of representative RNA sequences derived from the MD simulations that hybrid with C60 in the GC:AU, GC:GC and terminal regions, respectively.

Table 2. Calculation of binding free energy for dynamics hybridization of C60 with DNA/RNA

Nucleic acid	Binding modes	Starting identified sites	System	E_{vdW}		G_{solv}		G_{tot}	
				Mean (kcal mol^{-1})	Standard deviation	Mean (kcal mol^{-1})	Standard deviation	Mean (kcal mol^{-1})	Standard deviation
DNA	dsDNA twist	GC:GC:AT	1XRW	−34.26	3.55	9.21	1.01	−25.05	3.03
		AT:AT:AT	378D	−39.50	5.13	7.93	1.13	−31.56	4.27
	dsDNA unwinding	GC:GC:AT	1CP8	−31.55	5.51	7.86	0.84	−23.69	5.35
		GC:GC:AT	1I5V	−30.88	1.91	8.19	0.93	−22.69	1.78
	dsDNA stability	AT:AT:GC	108D	−40.60	2.52	7.85	0.57	−32.75	2.39
		GC:GC:AT	2ADW	−68.66	2.31	13.01	1.06	−55.65	2.23
	G-quadruplex disruption	–	2JT7	−51.38	3.16	10.89	1.07	−40.49	2.58
		–	1O0K	−45.89	2.97	6.49	0.60	−39.40	2.82
RNA	dsRNA curling	GC:AU:GC	1AKX	−33.73	4.34	13.04	1.75	−20.69	3.32
		GC:GC:GC	1ARJ	−55.98	3.21	21.17	1.78	−34.81	2.63
	Stabilized riboswitch	–	3NPB	−65.34	2.68	18.08	1.00	−47.27	2.74
		–	2GIS	−66.74	4.07	17.36	1.08	−49.38	4.02
	dsRNA stability	GC:GC:AU	2A04	−31.82	1.89	15.27	1.56	−16.55	1.58
		AU:AU:GC	2JUK	−20.05	4.96	9.82	1.32	−10.23	3.95

CONCLUSIONS

In this study, we have investigated the static and dynamic hybridization properties of C60 with DNA/RNA, and analyzed the potential toxic effects of the nanomolecule. Using statistical survey, MD simulations and thermodynamic analyses, we have found that:

(1) In the C60–dsDNA hybrids, C60 prefers the minor grooves of dsDNA involving three consecutive GC base pairs (GC_3), and the major grooves with three consecutive AT base pairs (AT_3). The presence of the base pair AT in the binding sites plays a key role in determining the groove binding specificity of C60.
(2) In the C60–dsRNA hybrids, C60 prefers the GC-rich regions of RNA, especially the GC-GC-AU sequences. More strikingly, the nanomolecule binds only to the major groove regions of RNA.
(3) The difference between the initial identified sites and the final stabilized sites implies that C60 initially binds to the initial identified sites of DNA/RNA to induce the structural changes of the nucleotides, such as DNA/RNA twist, unwinding and curling. Then, the C60 molecule moves to the final stabilized sites, which probably leads to potential toxic effects. This is similar to the process of food intake by mouth (initial) and then digestion in stomach (final).
(4) C60 hybridization enables to trigger the initiation of dsDNA unwinding, which probably inhibits the DNA discontinuous replication.
(5) C60 enables to disrupt the structure of G-quadruplex DNA, and thereby provides a possibility to activate the telomerase by facilitating its access to telomeres and in this way promotes the proliferation of tumor cells.
(6) C60 induces the conformational transition of HIV TAR RNA sequences from the stretch state to the curling state, which probably inhibits the HIV reverse transcription and represses the expression of HIV.
(7) C60 binds to the substrate-binding site of riboswitch RNA, showing great potential to be a new type of riboswitch substrate to regulate the gene expression.
(8) The nucleotides in the dsDNA stability, G-quadruplex disruption and stabilized riboswitch modes display much higher binding affinities to C60 than those in other modes, mainly due to the significant movement of C60, such as sliding.

SUPPLEMENTARY DATA

Supplementary Data are available at NAR Online.

ACKNOWLEDGEMENTS

Authors are grateful to Dr X.Z.Z. (Benkeman insititue, US) for English improvement.

FUNDING

High-Performance Computing Platform of Northwest A&F University, and is financially supported by the National Natural Science Foundation of China [31170796] and also the Fund of Northwest A&F University. Funding for open access charge: The National Natural Science Foundation of China (NSFC) is an organization directly affiliated to the State Council for the management of the National Natural Science Fund. And Northwest A&F University manages the Fund of Northwest A&F University.

Conflict of interest statement. None declared.

REFERENCES

1. Hess,H. and Tseng,Y. (2007) Active intracellular transport of nanoparticles: opportunity or threat? *ACS Nano*, **1**, 390–392.
2. Zuo,G., Huang,Q., Wei,G., Zhou,R. and Fang,H. (2010) Plugging into proteins: poisoning protein function by a hydrophobic nanoparticle. *ACS Nano*, **4**, 7508–7514.
3. Calzolai,L., Franchini,F., Gilliland,D. and Rossi,F.O. (2010) Protein–nanoparticle interaction: identification of the ubiquitin–gold nanoparticle interaction Site. *Nano Lett.*, **10**, 3101–3105.

4. Xu,X., Li,R., Ma,M., Wang,X., Wang,Y. and Zou,H. (2012) Multidrug resistance protein P-glycoprotein does not recognize nanoparticle C60: experiment and modeling. *Soft Matter*, **8**, 2915–2923.
5. Calvaresi,M. and Zerbetto,F. (2010) Baiting proteins with C60. *ACS Nano*, **4**, 2283–2299.
6. Tu,X., Manohar,S., Jagota,A. and Zheng,M. (2009) DNA sequence motifs for structure-specific recognition and separation of carbon nanotubes. *Nature*, **460**, 250–253.
7. Roxbury,D., Jagota,A. and Mittal,J. (2011) Sequence-specific self-stitching motif of short single-stranded DNA on a single-walled carbon nanotube. *J. Am. Chem. Soc.*, **133**, 13545–13550.
8. Xiao,Z., Wang,X., Xu,X., Zhang,H., Li,Y. and Wang,Y. (2011) Base- and structure-dependent DNA dinucleotide–carbon nanotube interactions: molecular dynamics simulations and thermodynamic analysis. *J. Phys. Chem. C*, **115**, 21546–21558.
9. Zhao,X., Striolo,A. and Cummings,P.T. (2005) C60 binds to and deforms nucleotides. *Biophys. J.*, **89**, 3856–3862.
10. Humphrey,W., Dalke,A. and Schulten,K. (1996) VMD: visual molecular dynamics. *J. Mol. Graphics*, **14**, 33–8, 27–28.
11. Schneidman-Duhovny,D., Inbar,Y., Nussinov,R. and Wolfson,H.J. (2005) PatchDock and SymmDock: servers for rigid and symmetric docking. *Nucleic Acids Res.*, **33**, W363–W367.
12. Lindahl,E., Hess,B. and van der Spoel,D. (2001) GROMACS 3.0: a package for molecular simulation and trajectory analysis. *J. Mol. Model.*, **7**, 306–317.
13. MacKerell,A.D., Bashford,D., Bellott,M., Dunbrack,R.L., Evanseck,J.D., Field,M.J., Fischer,S., Gao,J., Guo,H., Ha,S. *et al.* (1998) All-atom empirical potential for molecular modeling and dynamics studies of proteins. *J. Phys. Chem. B*, **102**, 3586–3616.
14. Mackerell,A.D. Jr, Feig,M. and Brooks,C.L. (2004) Extending the treatment of backbone energetics in protein force fields: limitations of gas-phase quantum mechanics in reproducing protein conformational distributions in molecular dynamics simulations. *J. Comput. Chem.*, **25**, 1400–1415.
15. Berendsen,H.J.C., Grigera,J.R. and Straatsma,T.P. (1987) The missing term in effective pair potentials. *J. Phys. Chem.*, **91**, 6269–6271.
16. Hoover,W.G. (1985) Canonical dynamics: equilibrium phase-space distributions. *Phys. Rev. A*, **31**, 1695–1697.
17. Parrinello,M. and Rahman,A. (1980) Crystal structure and pair potentials: a molecular-dynamics study. *Phys. Rev. Lett.*, **45**, 1196–1199.
18. Berk,H., Henk,B., Herman,J.C.B. and Johannes,G.E.M.F. (1997) LINCS: a linear constraint solver for molecular simulations. *J. Comput. Chem.*, **18**, 1463–1472.
19. Darden,T., York,D. and Pedersen,L. (1993) Particle mesh Ewald: an N.log(N) method for Ewald sums in large systems. *J. Chem. Phys.*, **98**, 10089–10092.
20. Hawkins,G.D., Cramer,C.J. and Truhlar,D.G. (1995) Pairwise solute descreening of solute charges from a dielectric medium. *Chem. Phys. Lett.*, **246**, 122–129.
21. Hawkins,G.D., Cramer,C.J. and Truhlar,D.G. (1996) Parametrized models of aqueous free energies of solvation based on pairwise descreening of solute atomic charges from a dielectric medium. *J. Phys. Chem.*, **100**, 19824–19839.
22. Dill,K.A. (1997) Additivity principles in biochemistry. *J. Biol. Chem.*, **272**, 701–704.
23. Srinivasan,J., Cheatham,T.E., Cieplak,P., Kollman,P.A. and Case,D.A. (1998) Continuum solvent studies of the stability of DNA, RNA, and phosphoramidate−DNA helices. *J. Am. Chem. Soc.*, **120**, 9401–9409.
24. Rohs,R., West,S.M., Sosinsky,A., Liu,P., Mann,R.S. and Honig,B. (2009) The role of DNA shape in protein-DNA recognition. *Nature*, **461**, 1248–1253.
25. Chargaff,E. and Davidson,J.N. (1955) *The Nucleic Acids: Chemistry and Biology*. Academic Press, New York.
26. Ogawa,T. and Okazaki,T. (1980) Discontinuous DNA replication. *Annu. Rev. Biochem.*, **49**, 421–457.
27. Tse,W.C. and Boger,D.L. (2004) Sequence-selective DNA recognition: natural products and nature's lessons. *Chem. Biol.*, **11**, 1607–1617.
28. Neidle,S. (1999) *Oxford Handbook of Nucleic Acid Structure*. Oxford University Press, Oxford, New York.
29. Mergny,J.L. and Helene,C. (1998) G-quadruplex DNA: a target for drug design. *Nat. Med.*, **4**, 1366–1367.
30. Richter,S., Ping,Y.-H. and Rana,T.M. (2002) TAR RNA loop: a scaffold for the assembly of a regulatory switch in HIV replication. *Proc. Natl. Acad. Sci. USA*, **99**, 7928–7933.
31. Toulme,J.J., Di Primo,C. and Moreau,S. (2001) Modulation of RNA function by oligonucleotides recognizing RNA structure. *Prog. Nucleic Acid Res. Mol. Biol.*, **69**, 1–46.
32. Montange,R.K. and Batey,R.T. (2008) Riboswitches: emerging themes in RNA structure and function. *Annu. Rev. Biophys.*, **37**, 117–133.
33. Lu,C., Ding,F., Chowdhury,A., Pradhan,V., Tomsic,J., Holmes,W.M., Henkin,T.M. and Ke,A. (2010) SAM recognition and conformational switching mechanism in the *Bacillus subtilis* yitJ S Box/SAM-I Riboswitch. *J. Mol. Biol.*, **404**, 803–818.
34. Yakovchuk,P., Protozanova,E. and Frank-Kamenetskii,M.D. (2006) Base-stacking and base-pairing contributions into thermal stability of the DNA double helix. *Nucleic Acids Res.*, **34**, 564–574.